ACS OMEGA

http://pubs.acs.org/journal/acsodf

Article

Structure and Properties of PVDF/PA6 Blends Compatibilized by Ionic Liquid-Grafted PA6

Xin Zheng, Yongjin Li,* Juntao Tang, and Guipeng Yu*

Cite This: *ACS Omega* 2022, 7, 12772−12778

Read Online

ACCESS | Metrics & More | Article Recommendations | Supporting Information

ABSTRACT: Compatibilization of immiscible blends is critically important for developing high-performance polymer materials. In this work, an ionic liquid, 1-vinyl-3-butyl imidazole chloride, grafted polyamide 6 (PA6-g-IL(Cl)) with a quasi-block structure was used as a compatibilizer for an immiscible poly(vinylidene fluoride) (PVDF)/PA6 blend. The effects of two PA6-g-IL(Cl)s (E-2%-50K and E-8%-50K) on the morphology, crystallization behavior, mechanical properties, and surface resistance of the PVDF/PA6 blend were investigated systematically. It was found that the two types of PA6-g-IL(Cl)s had a favorable compatibilization effect on the PVDF/PA6 blend. Specifically, the morphology of the PVDF/PA6 = 60/40 blend transformed from a typical sea-island into a bicontinuous structure after incorporating E-8%-50K with a high degree of grafting (DG). In addition, the tensile strength of the PVDF/PA6/E-8%-50K blend reached 66 MPa, which is higher than that of PVDF, PA6 and the PVDF/PA6 blend. Moreover, the PVDF/PA6/E-8%-50K blend exhibited surface conductivity due to the conductive path offered by the bicontinuous structure and conductive ions offered by grafted IL(Cl). Differential scanning calorimetry (DSC) and wide-angle X-ray diffractometry (WAXD) results revealed that PA6-g-IL(Cl) exhibits different effects on the crystallization behavior of PVDF and PA6. The compatibilization mechanism was concluded to be based on the fact that the nongrafted PA6 blocks entangled with the PA6 chains, while the ionic liquid-grafted PA6 blocks interacted with the PVDF chains. This work offers a new strategy for the compatibilization of immiscible polymer blends.

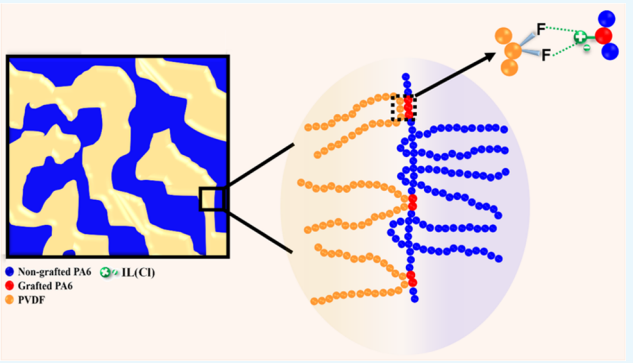

1. INTRODUCTION

Polymer blending is an effective and economic way to fabricate high-performance polymer materials to synergistically combine the properties of the different constituents.[1−3] The structure and properties of the multiphase polymer blends critically depend on the interfacial interaction. Compatibilizers are often required to enhance the interfacial adhesion for immiscible polymer blends.[4−6] From the principle of functionalization, the compatibilizers could be divided into two catalogs, i.e., nonreactive compatibilizers and reactive compatibilizers.[7,8] Generally, the nonreactive compatibilizers refer to block copolymers, which have at least two kinds of chemically distinct segments on one polymer chain. A typical block copolymer compatibilizer consists of the same segments as the immiscible blends or the segments that can interact with the components in immiscible blends. During melt processing, the block copolymer compatibilizer would migrate to the interface and reduce the interfacial tension, leading to enhanced compatibility.[9] The compatibilization efficiency of the block copolymer was dominated by its molecular and texture structure, such as the length of segments, number of blocks, and stacking mode of the compatibilizer and polymer matrix or other components.[10] Therefore, it is an ideal strategy to compatibilize the immiscible blends by incorporating a small amount of the block copolymer with task-specific designed blocks.

However, the preparation of the block copolymer is limited to living or controlled polymerization under harsh reaction conditions, which inevitably limit its applications in the industrial field.[11−13] Therefore, "quasi-block" copolymers prepared under mild conditions have been attracted much attention recently.[14−18] Guerrero-Sanchez et al. reported a versatile approach to the preparation of quasi-diblock copolymer libraries via a sequential reversible addition−fragmentation chain transfer polymerization (RAFT) method.[15] In our previous work, we have disclosed a convenient strategy to prepare quasi-block copolymers under mild conditions without a solvent.[19−21] Specifically, an ionic liquid (1-vinyl-3-butyl imidazole chloride, IL (Cl)) was grafted on poly(vinylidene fluoride) (PVDF) segments, which are located

Received: December 28, 2021
Accepted: March 30, 2022
Published: April 8, 2022

https://doi.org/10.1021/acsomega.1c07341
ACS Omega 2022, 7, 12772−12778

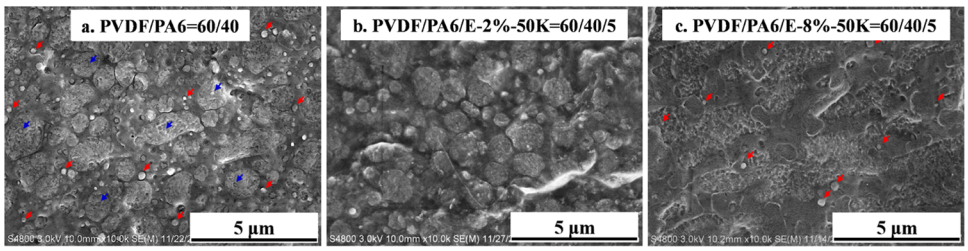

Figure 1. SEM images of the fractured surface for (a) PVDF/PA6 blend, (b) PVDF/PA6/E-2%-50K blend, and (c) PVDF/PA6/E-8%-50K blend.

in an amorphous region through radiation-induced in situ grafting method.[21] The ionic liquid-grafted PVDF segments separated from nongrafted PVDF segments during heating, implying different physical properties of the two "blocks".[20] Similarly, IL(Cl)-grafted polyamide 6 (PA6) (PA6-g-IL(Cl)) was prepared using the aforementioned method.[22,23] Also, the quasi-block structure and property were expected for the prepared PA6-g-IL(Cl).

On the other hand, significant attention has been paid mainly to the phase behaviors of the synthesized quasi-block copolymers.[16,21,24] We considered that such quasi-block copolymers are also the good candidates as compatibilizers for immiscible polymer blends because of the blocky architecture. To verify the compatibilization effect of PA6-g-IL(Cl), an immiscible PVDF/PA6 blend was chosen representatively. On the one hand, it is important to compatibilize the PVDF/PA6 blend because the immiscibility may exert an adverse influence on its application in the fuel cell environment.[25] On the other hand, PVDF and PA6 were expected to interact with the "blocks" of PA6-g-IL(Cl) separately. In this work, two kinds of PA6-g-IL(Cl), E-2%-50K and E-8%-50K, with different degrees of grafting (DG) were applied. The effects of E-2%-50K and E-8%-50K on the structure and properties of the PVDF/PA6 blend were investigated systematically. To our best knowledge, it is the first time that the idea of using this kind of quasi-block copolymer as a compatibilizer is put forward.

2. EXPERIMENTAL SECTION

2.1. Materials. Polyamide 6 (PA6) (UBE Nylon 1022B) with a density of 1.14 g/cm^3 and a melting temperature of 215−225 °C was purchased from UBE Industries Ltd. in Japan. Poly(vinylidene fluoride) (PVDF) with commercial name KF850 (M_w = 2.09 × 10^5, M_w/M_n = 2) was supplied by Kureha Chemicals in Tokyo, Japan. The ionic liquid, 1-vinyl-3-butyl imidazole chloride (IL(Cl)) (M_m = 187 g/mol) was produced by Lanzhou Yulu Fine Chemical Co., Ltd.

2.2. Preparation of PA6-g-IL(Cl). The preparation of PA6-g-IL(Cl) was described in our previous work at length,[22] which can also be found in the Supporting Information. The PA6-g-IL(Cl) with a degree of grafting (DG) of 1.4% (E-2%-50K) and 7.8% (E-8%-50K) was employed as a compatibilizer in this work. The solid-state NMR spectrum and the total ion chromatogram of E-8%-50K are shown in Figures S1 and S2. New peaks in the NMR spectrum and characteristic fragments of the ionic liquid in the total ion chromatogram confirmed the formation of PA6-g-IL(Cl).

2.3. Preparation of PVDF/PA6/PA6-g-IL(Cl) Blends. All raw materials were dried thoroughly in a vacuum oven before melt-mixing. The PVDF/PA6 = 60/40 blend and the PVDF/PA6/PA6-g-IL(Cl) = 60/40/5 blend were prepared on a Haake Polylab QC mixer equipped with a twin-screw. In practice, an extra 5% of PA6 was added in the PVDF/PA6 = 60/40 binary blend to balance the addition of PA6-g-IL(Cl) in the compatibilized blend. All blends were sheared at 20 rpm for 2 min followed by 50 rpm for 5 min at 230 °C.

The films of the PVDF/PA6 blend and the PVDF/PA6/PA6-g-IL(Cl) blend were formed by hot-pressing at 240 °C under 10 MPa pressure followed by cooling at the same pressure. The films were used for characterizations directly.

2.4. Characterizations. The microstructure of the fractured surface of samples was observed using a field emission scanning electron microscope (SEM, Hitachi S-4800). The samples were fractured in liquid nitrogen followed by coating with gold before observation. An acceleration voltage of 3 kV was used for sample observation.

Mechanical properties were determined using an Instron universal material testing blend (model 5966) at room temperature. The tensile speed was 5 mm/min. The specimens were prepared by injection molding according to ISO 527-2-5A.

The notched impact strength was tested on an impact testing machine (SS-3700CZ) equipped with a 4 J of pendulum according to GB/T 16420-1996. The specimens for the impact test were prepared by injection molding according to GB/T 1043.

The Fourier transform infrared (FTIR) spectroscopy measurements were conducted on film samples with a transmittance mode using an FTIR spectrometer (Bruker Vertex 70V). FTIR spectra were recorded from 4000 to 400 cm^{-1} at a resolution of 2 cm^{-1}, and 64 scans were averaged.

A wide-angle X-ray diffractometer (WAXD, Bruker-D8) was used to detect the crystalline forms of the samples. The data were collected from 5 to 40 ° at a scanning speed of 1 °/min. The step interval was 0.02 °.

Differential scanning calorimetric (DSC, TA-Q2000) measurements were used to track the crystallization and melting behaviors of all samples under a high-purity nitrogen atmosphere. All samples were heated to 250 °C and held for 5 min to erase thermal history, then cooled to 20 °C, followed by heating again to 250 °C. Both the cooling and heating rate were 10 °C/min. The first cooling and second heating curves were recorded.

Electrical conductivity was measured on an ultrahigh resistivity meter (MCP-HT450). The URS probe electrode and 10 V were adopted to test the electrical conductivity. The thickness of the samples was about 500 μm.

The small-amplitude shear oscillation (SAOS) measurements were carried out on a physical rheometer (MCR301, Anton Paar Instrument). The diameter of both parallel plates was 25 mm. The gap between the two plates was 1 mm. The experiments were carried out at 235 °C in a nitrogen atmosphere. The frequencies were ranged from 0.1 to 100 rad/s. The strain amplitude was 1%.

https://doi.org/10.1021/acsomega.1c07341
ACS Omega 2022, 7, 12772−12778

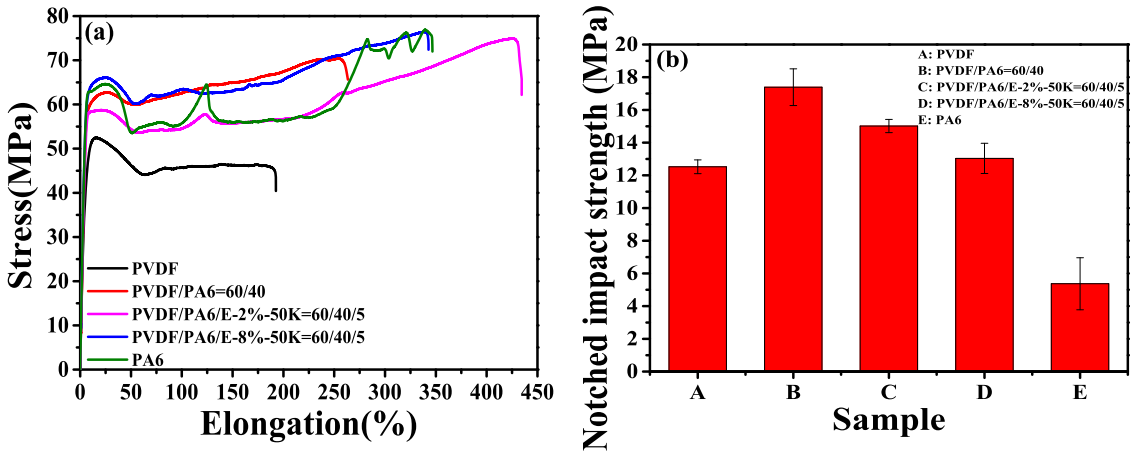

Figure 2. Mechanical properties of PVDF, PA6, PVDF/PA6 blends, and PVDF/PA6/PA6-g-IL(Cl) blends: (a) stress−strain curves and (b) notched impact strength.

Table 1. Summary of Mechanical Properties of Samples Shown in Figure 2

sample	yield strength (MPa)	elongation at break (%)	modulus (MPa)
PVDF	52.5 ± 0.7	192.1 ± 1.8	1278.1 ± 20.2
PVDF/PA6 = 60/40	62.8 ± 3.2	263.7 ± 12.3	1494.7 ± 11.4
PVDF/PA6/E-8%-50K = 60/40/5	66.2 ± 1.8	342.5 ± 11.5	1494.6 ± 38.8
PVDF/PA6/E-2%-50K = 60/40/5	58.7 ± 1.5	435.4 ± 20.6	1252.1 ± 25.7
PA6	63.0 ± 1.4	347.0 ± 1.3	1258.7 ± 27.6

Table 2. Surface Resistivity of PVDF, PA6, PVDF/PA6 Blends, and PVDF/PA6/PA6-g-IL(Cl) Blends

sample	PVDF	PVDF/PA6 = 60/40	PVDF/PA6/E-8%-50K = 60/40/5	PA6
surface resistance (Ω)	over	4.33×10^{12}	2.60×10^{11}	3.83×10^{12}

3. RESULTS AND DISCUSSION

3.1. Morphology. The compatibilization effect of quasi-block PA6-g-IL(Cl) on a PVDF/PA6 blend was demonstrated by SEM images (Figure 1). A typical sea-island microstructure was recognized for the PVDF/PA6 = 60/40 blend, where PA6 is the matrix and PVDF forms the domains (Figure 1a). Note that there are PVDF nanodomains (marked with red arrows) in the PA6 matrix and PA6 nanodomains (marked with blue arrows) in PVDF domains. With the incorporation of quasi-block E-2%-50K with lower DG, the interface between PA6 and PVDF became ambiguous (Figure 1b), and the nanodomains coalesced, indicating improved interface adhesion. However, the sea-island microstructure was still observed, implying a limited compatibilization effect. This was ascribed to the relative low DG of quasi-block E-2%-50K. The conclusion was further proved by adding E-8%-50K with higher DG to the PVDF/PA6 blend. As shown in Figure 1c, the morphology of the E-8%-50K compatibilized blend changed from a sea-island to a bicontinuous structure. Obviously, E-8%-50K with higher DG has a better compatibilization effect than that of E-2%-50K. The compatibilization of E-8%-50K on the PVDF/PA6 = 20/80 blend was also examined. The morphology and mechanical and rheological properties of the E-8%-50K compatibilized PVDF/PA6 = 20/80 blend are provided in Figures S3 and S4. The decreased PVDF domain size, the increased mechanical properties, and the increased storage modulus and complex viscosity revealed that the PA6-g-IL(Cl) also has a good compatibilization effect on the PVDF/PA6 = 20/80 blend.

3.2. Mechanical Properties. The mechanical properties of PA6-g-IL(Cl) compatibilized PVDF/PA6 blends were evaluated by tensile and impact tests, and the results are shown in Figure 2. Neat PVDF, PA6, and PVDF/PA6 blends were tested at the same time as comparisons. Detailed mechanical properties based on Figure 2a are summarized in Table 1. Obviously, PA6 exhibited high strength, modulus, and ductility and low notched impact strength. On the contrary, the strength, modulus, and ductility of PVDF were lower, but the impact strength was much higher than that of PA6. The combination of PVDF and PA6 showed good mechanical properties, as shown in Figure 2. This was due to the inherent interactions between PVDF and PA6. With the incorporation of E-2%-50K, the strength and the modulus decreased but the elongation increased compared to the PVDF/PA6 binary blend. However, the yield strength of the PVDF/PA6 blend increased to 66.2 MPa as E-8%-50K was incorporated. In addition, the quasi-block E-8%-50K compatibilized PVDF/PA6 blend exhibited a modulus as high as the PVDF/PA6 binary blend. The enhancement in tensile properties of the PVDF/PA6/E-8%-50K = 60/40/5 blend was ascribed to the bicontinuous microstructure. As shown in Figure 2b, the PVDF/PA6 binary blend exhibited the highest notched impact strength, while the quasi-block PA6-g-IL(Cl) compatibilized PVDF/PA6 blends showed decreased notched impact strength as the DG increased. It is expected that the compatibilization effect of quasi-block PA6-g-IL(Cl) made the blends more uniform, leading to averaged properties over the components. However, it is notable that the notched impact strength of

https://doi.org/10.1021/acsomega.1c07341
ACS Omega 2022, 7, 12772−12778

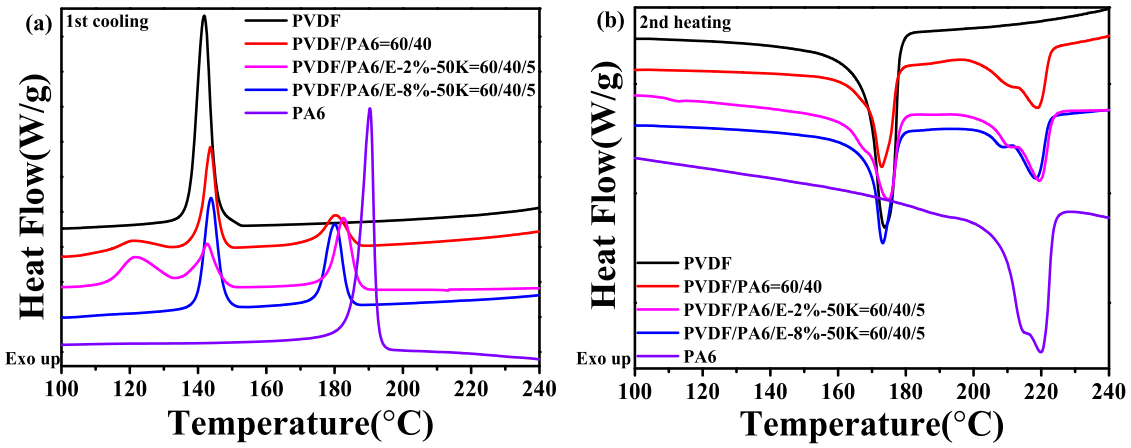

Figure 3. Crystallization (1st cooling) (a) and melting (2nd heating) (b) curves of PVDF, PA6, PVDF/PA6 blends, and PVDF/PA6/PA6-g-IL(Cl) blends.

Table 3. Crystallization Parameters of Samples Shown in Figure 3

sample	$T_{m,PVDF}$ (°C)	$T_{m,PA6}$ (°C)	$T_{c,PVDF}$ (°C)	$T_{c,PA6}$ (°C)	$\chi_{c,PVDF}$ (%)	$\chi_{c,PA6}$ (%)
PVDF	173.7		141.8		61.0	
PVDF/PA6 = 60/40	172.9	219.1	120.4, 143.6	180.4	55.8	25.4
PVDF/PA6/E-2%-50K = 60/40/5	174.7	219.3	121.5, 142.7	182.7	56.1	25.7
PVDF/PA6/E-8%-50K = 60/40/5	173.2	218.8	143.7	180.0	67.8	19.3
PA6		219.6		190.4		27.3

PVDF/PA6/PA6-g-IL(Cl) blends was still higher than that of neat PVDF and PA6.

3.3. Surface Resistance. The surface resistance of all samples is presented in Table 2. Obviously, the neat PVDF is an insulating polymer, with a high surface resistance that is out of the testing range. PA6 also exhibits insulative properties, while the adsorption of water helps to dissipate the accumulated static electricity. This explains the poor antistatic properties of PVDF/PA6 binary blends, which were maintained at a range of 10^{12} Ω. However, the surface resistivity of PVDF/PA6/E-8%-50K = 60/40/5 reduced to a level of 10^{11} Ω. The quasi-block PA6-g-IL was responsible for the enhanced surface resistance. On the one hand, the bicontinuous structure of PVDF/PA6/E-8%-50K = 60/40/5 offered the conductivity path; on the other hand, though cations of the ionic liquid were grafted on a PA6 molecular chain, the anions of the ionic liquid were free and acted as conductivity ions.

3.4. Crystallization Behaviors. Figure 3 exhibits the DSC curves of a quasi-block PA6-g-IL(Cl) compatibilized PVDF/PA6 blend as well as neat PVDF and PA6. Table 3 demonstrates the crystallization (T_c) and melting (T_m) temperatures and the crystallinities of PVDF ($\chi_{c,\ PVDF}$) and PA6 ($\chi_{c,\ PA6}$) in all samples. The crystallinity was calculated according to formula 1 as follows:

$$\chi_c = \frac{\Delta H_m}{\phi \times \Delta H_m^0} \times 100\% \quad (1)$$

where ΔH_m is the melting enthalpy of specified components, ϕ is the weight ratio of specified components, and ΔH_m^0 is the theoretical melting enthalpy of 100% crystalline components, with a value of 104.5[26−28] and 190 J/g[29,30] for PVDF and PA6, respectively.

As shown in Figure 3a, only one strong crystallization peak with a narrow half-peak breadth was observed for both PVDF and PA6, indicating the strong crystallization capability of PVDF and PA6. Interestingly, in the binary blend of PVDF/PA6 = 60/40 blend, three crystallization peaks were recognized. However, according to Figure 3b, there were only two melting peaks correspondingly for the PVDF/PA6 binary blend. This implied two kinds of crystals generated during crystallization. The peak located at 180.4 °C was assigned to the crystallization of the PA6 matrix, which was lower than that of neat PA6 (190.4 °C). This may be related to the inherent interaction between PVDF and PA6.[19] The peak around 143.6 °C was ascribed to the crystallization of PVDF domains. Whereas, the broad crystallization peak at 120.4 °C may result from the confined crystallization of nanosized PVDF domains, which was pointed out by the red arrow in Figure 1a.

Though quasi-block E-2%-50K exhibited a limited compatibilization effect on a PVDF/PA6 blend according to Figure 1b, the crystallization and melting behaviors of the PVDF/PA6/E-2%-50K = 60/40/5 blend did not change much compared to those of the PVDF/PA6 = 60/40 blank control. There were also three crystallization peaks of the PVDF/PA6/E-2%-50K = 60/40/5 blend. In addition, the crystallinity of PVDF and PA6 components in the E-2%-50K compatibilized blend were almost the same as that in the PVDF/PA6 = 60/40 blend.

Whereas, in a quasi-block E-8%-50K compatibilized PVDF/PA6 blend, only two melting peaks appeared. One peak was assigned to crystalline melting of PVDF at lower temperature, and the other one peak was attributed to that of PA6 at higher temperature. The confined crystallization peak of PVDF disappeared, which was in good accordance with the microstructure exhibited in Figure 1c. In addition, though the crystallization and melting temperatures of PVDF and PA6 components in the quasi-block E-8%-50K compatibilized PVDF/PA6 blend were almost the same as those in the PVDF/PA6 = 60/40 blank control, the crystallinity of PVDF

https://doi.org/10.1021/acsomega.1c07341
ACS Omega 2022, 7, 12772−12778

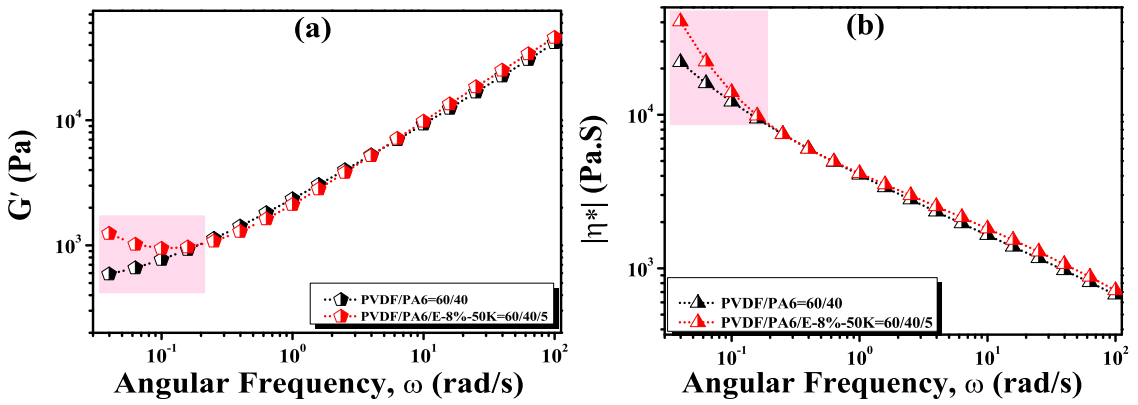

Figure 4. Rheological properties of the PVDF/PA6 blend and the PVDF/PA6/E-8%-50K blend: (a) storage modulus G' and (b) complex viscosity $|\eta^*|$ as functions of angular frequency.

increased and the crystallinity of PA6 decreased at the same time. This may be attributed to the fact that the quasi-block E-8%-50K has different effect on PA6 and PVDF phases. Specifically, the nongrafted PA6 blocks in quasi-block E-8%-50K entangled with the PA6 phase when cooling down from the melt, the nongrafted PA6 blocks participated in crystallization, while the grafted PA6 blocks were expelled from the crystal, bringing crystal defect to the PVDF/PA6 interface and leading to decreased PA6 crystallinity. On the other hand, the imidazolium cations on grafted PA6 blocks may interact with $-CF_2$ in PVDF, which might affect the crystalline behavior of PVDF significantly. The different effects of PA6-g-IL on the crystallization of PVDF and PA6 also revealed the compatibilization mechanism, which will be further investigated via FTIR and WAXD.

3.5. Compatibilization Mechanism. The effect of PA6-g-IL(Cl) on PVDF/PA6 blends was investigated by SEM, DSC, tensile test, and impact test. Results showed that the PA6-g-IL(Cl), especially E-8%-50K with high DG, exhibited an obvious compatibilization effect. According to the rheological properties shown in Figures 4 and S4, higher G' and $|\eta^*|$ were observed for the E-8%-50K compatibilized PVDF/PA6 blends in the low-frequency region compared to the corresponding PVDF/PA6 binary blend. This indicated stronger interactions in the compatibilized blends due to the incorporation of PA6-g-IL(Cl). The unique interactions will be further discussed in this section.

According to the FTIR spectra given in Figure S5, the polar $-CF_2$ group in PVDF interacted with the amide groups in the PA6 matrix; no obvious peaks of quasi-block PA6-g-IL(Cl) were observed in PVDF/PA6/PA6-g-IL(Cl) blends. In addition, only the featured PVDF peaks of α phase crystals were observed for PVDF/PA6 and PVDF/PA6/PA6-g-IL(Cl) blends. This implied that the grafted ionic liquid on quasi-block PA6-g-IL(Cl) cannot induce the polar γ crystals of PVDF, which is different from the results reported in our previous work.[31] To further investigate the effect of the grafted ionic liquid on the crystallization of PVDF, WAXD was applied to examine the crystalline structure. The WAXD patterns are given in Figure 5. The assignment of main peaks in neat PVDF and PA6 was done according to the literature.[22,31−33] In the PVDF/PA6 blends with and without quasi-block PA6-g-IL(Cl), a preferred orientation worth noting was observed. The effect of quasi-block PA6-g-IL(Cl) on the preferred orientation of PVDF was the main focus. The relative intensity ratios of the [100α] peak (marked as "A") to other peaks

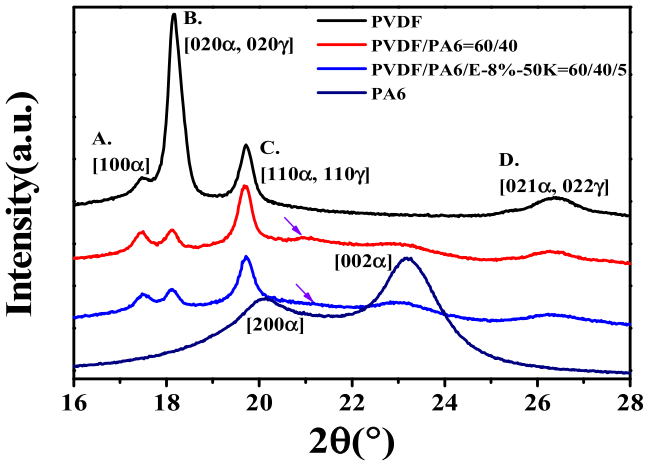

Figure 5. XRD patterns of PVDF, PA6, PVDF/PA6 blends, and PVDF/PA6/E-8%-50K blends. A, B, C, and D are the characteristic peaks of PVDF.

(marked as "B", "C", and "D") in all blends were calculated and are shown in Table 4. Since no obvious PVDF γ phase crystals

Table 4. Relative Intensity Ratios of PVDF Peaks

sample	PVDF	PVDF/PA6 = 60/40	PVDF/PA6/E-8%-50 = 60/40/5
I_A/I_B	0.64	0.99	0.98
I_A/I_C	0.90	0.85	0.86
I_A/I_D	1.07	1.08	1.09

were identified from the FTIR spectra shown in Figure S5, and the peak intensity of the PVDF [100α] plane did not show a significant change in all samples, the decreased value of I_A/I_B was mainly ascribed to the restricted growth of the PVDF [020α] plane with the incorporation of PA6. However, the restriction effect was not obvious with the addition of quasi-block PA6-g-IL(Cl), as the value of I_A/I_B was smaller than that in PVDF/PA6 binary blends. This means that the grafted PA6 blocks promoted the growth of the PVDF [020α] plane slightly. It is reasonable to deduce that the interaction between the grafted ionic liquid and $-CF_2$ in PVDF promoted the growth of the PVDF [020α] plane. In addition, the values of I_A/I_C and I_A/I_D of PVDF/PA6/E-8%-50K blends were different from those of PVDF/PA6 binary blends, indicating the special effects of quasi-block PA6-g-IL(Cl) on the crystallization behavior of PVDF. Apart from that, there was

https://doi.org/10.1021/acsomega.1c07341
ACS Omega 2022, 7, 12772−12778

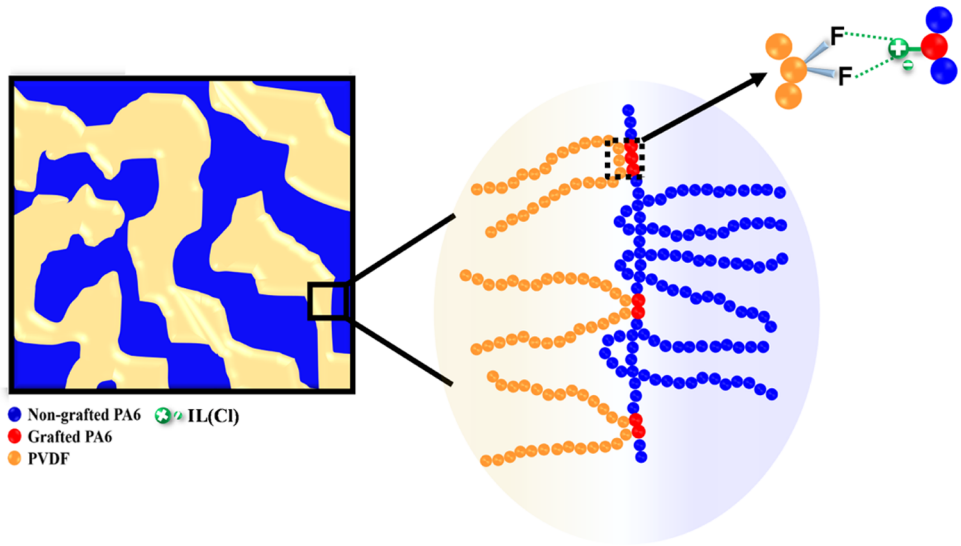

Figure 6. Quasi-block structure of PA6-g-IL(Cl) and its compatibilization effect on the PVDF/PA6 blend.

a weak peak that emerged in PVDF/PA6 binary blends at about 21 °, which was pointed with arrows and may be related to the generation of metastable γ phase crystals of the PA6 matrix. On the contrary, no new peak was observed at the corresponding location in PVDF/PA6/E-8%-50K blends, which may be due to the stronger interactions between PVDF and PA6 with PA6-g-IL(Cl) serving as compatibilizers. Based on the above analysis, it is concluded that the PA6-g-IL(Cl) increased the interface adhesion between the PVDF and PA6 phase, and the compatibilization effect of PA6-g-IL(Cl) showed an important influence on the crystallization process of both PVDF and PA6. The compatibilization mechanism is schematically shown in Figure 6.

4. CONCLUSIONS

A unique quasi-block structure of the ionic liquid-grafted polymer shows great potential in polymer compatibilization. In this work, an ionic liquid-grafted PA6 (PA6-g-IL(Cl)) was prepared and exhibited an obvious compatibilization effect by changing the morphology of an immiscible PVDF/PA6 blend from a sea-island to a bicontinuous structure. Specifically, the ionic liquid-grafted PA6 "blocks" interact with PVDF chains, while nongrafted PA6 "blocks" entangle with PA6 chains. The compatibilization mechanism was proved by the different effects of PA6-g-IL on the crystallization behavior of PVDF and PA6, respectively. PA6-g-IL showed an obvious advantage over traditional block copolymers with respect to the preparation process. Therefore, this work offered a new strategy and feasible way to prepare the quasi-block polymer and realize the compatibilization of an immiscible blend using the prepared quasi-block PA6-g-IL(Cl).

■ ASSOCIATED CONTENT

Supporting Information

The Supporting Information is available free of charge at https://pubs.acs.org/doi/10.1021/acsomega.1c07341.

Preparation method of PA6-g-IL(Cl); solid-state NMR spectra of PA6 and E-8%-50K; total ion current obtained from Py-GC/MS for PA6 and E-8%-50K; SEM fractured surface, stress−strain curves, and notched impact strength of the PVDF/PA6 = 20/80 blend and the PVDF/PA6/E-8%-50K = 20/80/5 blend; rheological properties of PVDF, PA6, PVDF/PA6 blend, and PVDF/PA6/E-8%-50K blend; and FTIR spectra of PVDF, PA6, PVDF/PA6 blend, and PVDF/PA6/E-8%-50K blend (PDF)

■ AUTHOR INFORMATION

Corresponding Authors

Yongjin Li − *Key Laboratory of Organosilicon Chemistry and Material Technology, Ministry of Education, College of Material, Chemistry and Chemical Engineering, Hangzhou Normal University, Hangzhou 311121 Zhejiang, People's Republic of China;* orcid.org/0000-0001-6666-1336; Email: yongjin-li@hznu.edu.cn

Guipeng Yu − *College of Chemistry and Chemical Engineering, Central South University, Changsha 410083, People's Republic of China;* orcid.org/0000-0001-8712-0512; Email: gilbertyu@csu.edu.cn

Authors

Xin Zheng − *College of Chemistry and Chemical Engineering, Central South University, Changsha 410083, People's Republic of China; Key Laboratory of Organosilicon Chemistry and Material Technology, Ministry of Education, College of Material, Chemistry and Chemical Engineering, Hangzhou Normal University, Hangzhou 311121 Zhejiang, People's Republic of China*

Juntao Tang − *College of Chemistry and Chemical Engineering, Central South University, Changsha 410083, People's Republic of China*

Complete contact information is available at: https://pubs.acs.org/10.1021/acsomega.1c07341

Author Contributions

X.Z. contributed to investigation, data analysis, writing—original draft, and funding acquisition; Y.L. contributed to conceptualization, discussion, project administration, and supervision; J.T. contributed to discussion and writing—review; and G.Y. contributed to writing—review and editing, discussion, and supervision.

https://doi.org/10.1021/acsomega.1c07341
ACS Omega 2022, 7, 12772−12778

Notes

The authors declare no competing financial interest.

■ ACKNOWLEDGMENTS

This work was financially supported by the National Natural Science Foundation of China (52103026).

■ REFERENCES

(1) Zhao, X.; Wang, H.; Fu, Z.; Li, Y. Enhanced interfacial adhesion by reactive carbon nanotubes: new route to high-performance immiscible polymer blend nanocomposites with simultaneously enhanced toughness, tensile strength, and electrical conductivity. *ACS Appl. Mater. Interfaces* **2018**, *10*, 8411−8416.
(2) Sui, G.; Jing, M.; Zhao, J.; Wang, K.; Zhang, Q.; Fu, Q. A comparison study of high shear force and compatibilizer on the phase morphologies and properties of polypropylene/polylactide (PP/PLA) blends. *Polymer* **2018**, *154*, 119−127.
(3) Li, Y.; Shimizu, H. Morphological investigations on the nanostructured poly (vinylidene fluoride)/polyamide 11 blends by high-shear processing. *Eur. Polym. J.* **2006**, *42*, 3202−3211.
(4) Fu, Z.; Wang, H.; Zhao, X.; Li, X.; Gu, X.; Li, Y. Flame-retarding nanoparticles as the compatibilizers for immiscible polymer blends: simultaneously enhanced mechanical performance and flame retardancy. *J. Mater. Chem. A* **2019**, *7*, 4903−4912.
(5) Wang, H.; Yang, X.; Fu, Z.; Zhao, X.; Li, Y.; Li, J. Rheology of nanosilica-compatibilized immiscible polymer blends: Formation of a "heterogeneous network" facilitated by interfacially anchored hybrid nanosilica. *Macromolecules* **2017**, *50*, 9494−9506.
(6) Seyni, F. I.; Grady, B. P. Janus particles as immiscible polymer blend compatibilizers: a review. *Colloid Polym. Sci.* **2021**, *299*, 585−593.
(7) Jandas, P. J.; Mohanty, S.; Nayak, S. K. Morphology and thermal properties of renewable resource-based polymer blend nanocomposites influenced by a reactive compatibilizer. *ACS Sustainable Chem. Eng.* **2014**, *2*, 377−386.
(8) Spontak, R. J.; Ryan, J. J. Polymer Blend Compatibilization by the Addition of Block Copolymers. In *Compatibilization of Polymer Blends*; Ajitha, A. R.; Thomas, S., Eds.; Academic Press, 2020; pp 57−102.
(9) Anastasiadis, S. H.; Gancarz, I.; Koberstein, J. T. Compatibilizing effect of block copolymers added to the polymer/polymer interface. *Macromolecules* **1989**, *22*, 1449−1453.
(10) Van Hemelrijck, E.; Van Puyvelde, P.; Macosko, C. W.; et al. The effect of block copolymer architecture on the coalescence and interfacial elasticity in compatibilized polymer blends. *J. Rheol.* **2005**, *49*, 783−798.
(11) Okubo, M.; Minami, H.; Zhou, J. Preparation of block copolymer by atom transfer radical seeded emulsion polymerization. *Colloid Polym. Sci.* **2004**, *282*, 747−752.
(12) Sun, J. T.; Hong, C. Y.; Pan, C. Y. Recent advances in RAFT dispersion polymerization for preparation of block copolymer aggregates. *Polym. Chem.* **2013**, *4*, 873−881.
(13) Kagawa, Y.; Minami, H.; Okubo, M.; et al. Preparation of block copolymer particles by two-step atom transfer radical polymerization in aqueous media and its unique morphology. *Polymer* **2005**, *46*, 1045−1049.
(14) Guerrero-Sanchez, C.; O'Brien, L.; Brackley, C.; Keddie, D. J.; Saubern, S.; Chiefari, J. Quasi-block copolymer libraries on demand via sequential RAFT polymerization in an automated parallel synthesizer. *Polym. Chem.* **2013**, *4*, 1857−1862.
(15) Haven, J. J.; Guerrero-Sanchez, C.; Keddie, D. J.; Moad, G. Rapid and systematic access to quasi-diblock copolymer libraries covering a comprehensive composition range by sequential RAFT polymerization in an automated synthesizer. *Macromol. Rapid Commun.* **2014**, *35*, 492−497.
(16) Lechuga-Islas, V. D.; Festag, G.; Rosales-Guzman, M.; Vega-Becerra, O. E.; Guerrero-Santos, R.; Schubert, U. S.; Guerrero-Sanchez, C. Quasi-block copolymer design of quaternized derivatives of poly (2-(dimethylamino) ethyl methacrylate): Investigations on thermo-induced self-assembly. *Eur. Polym. J.* **2020**, *124*, No. 109457.
(17) Weiss, E.; Daoulas, K. C.; Müller, M.; Shenhar, R. Quasi-block copolymers: design, synthesis, and evidence for their formation in solution and in the melt. *Macromolecules* **2011**, *44*, 9773−9781.
(18) Sanguramath, R. A.; Nealey, P. F.; Shenhar, R. Quasi-block copolymers based on a general polymeric chain stopper. *Chem. − Eur. J.* **2016**, *22*, 10203−10210.
(19) Xing, C.; Wang, Y.; Zhang, C.; et al. Immobilization of ionic liquids onto the poly (vinylidene fluoride) by electron beam irradiation. *Ind. Eng. Chem. Res.* **2015**, *54*, 9351−9359.
(20) Xing, C.; Li, J.; Yang, C.; et al. Local grafting of ionic liquid in poly (vinylidene fluoride) amorphous region and the subsequent microphase separation behavior in melt. *Macromol. Rapid Commun.* **2016**, *37*, 1559−1565.
(21) Guan, J.; Wang, Y.; Xing, C.; et al. Semicrystalline Polymer Binary-Phase Structure Templated Quasi-Block Graft Copolymers. *J. Phys. Chem. B* **2017**, *121*, 7508−7518.
(22) Zheng, X.; Ding, X.; Guan, J.; et al. Ionic liquid-grafted polyamide 6 by radiation-induced grafting: New strategy to prepare covalently bonded ion-containing polymers and their application as functional fibers. *ACS Appl. Mater. Interfaces* **2019**, *11*, 5462−5475.
(23) Zheng, X.; Chen, F.; Zhang, X.; et al. Ionic liquid grafted polyamide 6 as porous membrane materials: enhanced water flux and heavy metal adsorption. *Appl. Surf. Sci.* **2019**, *481*, 1435−1441.
(24) Daoulas, K. C.; Cavallo, A.; Shenhar, R.; Müller, M. Phase behaviour of quasi-block copolymers: A DFT-based Monte-Carlo study. *Soft Matter* **2009**, *5*, 4499−4509.
(25) Li, Y.; Shimizu, H. Conductive PVDF/PA6/CNTs nanocomposites fabricated by dual formation of cocontinuous and nanodispersion structures. *Macromolecules* **2008**, *41*, 5339−5344.
(26) Jang, J. W.; Min, B. G.; Yeum, J. H.; et al. Structures and physical properties of graphene/PVDF nanocomposite films prepared by solution-mixing and melt-compression. *Fibers Polym.* **2013**, *14*, 1332−1338.
(27) Teyssedre, G.; Bernes, A.; Lacabanne, C. Influence of the crystalline phase on the molecular mobility of PVDF. *J. Polym. Sci., Part B: Polym. Phys.* **1993**, *31*, 2027−2034.
(28) Mohamadi, S.; Sharifi-Sanjani, N. Investigation of the crystalline structure of PVDF in PVDF/PMMA/graphene polymer blend nanocomposites. *Polym. Compos.* **2011**, *32*, 1451−1460.
(29) Guo, B.; Zou, Q.; Lei, Y.; et al. Crystallization behavior of polyamide 6/halloysite nanotubes nanocompositesl. *Thermochim. Acta* **2009**, *484*, 48−56.
(30) Campoy, I.; Gomez, M. A.; Marco, C. Structure and thermal properties of blends of nylon 6 and a liquid crystal copolyester. *Polymer* **1998**, *39*, 6279−6288.
(31) Xing, C.; Zhao, M.; Zhao, L.; et al. Ionic liquid modified poly (vinylidene fluoride): crystalline structures, miscibility, and physical properties. *Polym. Chem.* **2013**, *4*, 5726−5734.
(32) Gregorio, R., Jr. Determination of the α, β, and γ crystalline phases of poly (vinylidene fluoride) films prepared at different conditions. *J. Appl. Polym. Sci.* **2006**, *100*, 3272−3279.
(33) Bose, S.; Bhattacharyya, A. R.; Kodgire, P. V.; et al. Fractionated crystallization in PA6/ABS blends: Influence of a reactive compatibilizer and multiwall carbon nanotubes. *Polymer* **2007**, *48*, 356−362.

https://doi.org/10.1021/acsomega.1c07341
ACS Omega 2022, 7, 12772−12778